

## WIYN OPEN CLUSTER STUDY. LIX. RADIAL-VELOCITY MEMBERSHIP OF THE EVOLVED POPULATION OF THE OLD OPEN CLUSTER NGC 6791

BENJAMIN M. TOFFLEMIRE,<sup>1,2</sup> NATALIE M. GOSNELL,<sup>1,2</sup> ROBERT D. MATHIEU,<sup>1,2</sup> AND IMANTS PLATAIS<sup>3</sup>

*Accepted to The Astronomical Journal July 28, 2014*

### ABSTRACT

The open cluster NGC 6791 has been the focus of much recent study due to its intriguing combination of old age and high metallicity ( $\sim 8$  Gyr,  $[\text{Fe}/\text{H}] = +0.30$ ), as well as its location within the *Kepler* field. As part of the WIYN Open Cluster Study, we present precise ( $\sigma = 0.38 \text{ km s}^{-1}$ ) radial velocities for proper-motion candidate members of NGC 6791 from Platais et al. Our survey, extending down to  $g' \sim 16.8$ , is comprised of the evolved cluster population, including blue stragglers, giants, and horizontal branch stars. Of the 280 proper-motion-selected stars above our magnitude limit, 93% have at least one radial-velocity measurement and 79% have three measurements over the course of at least 200 days, sufficient for secure radial-velocity-determined membership of non-velocity-variable stars. The Platais et al. proper-motion catalog includes twelve anomalous horizontal branch candidates blueward of the red clump, of which we find only four to be cluster members. Three fall slightly blueward of the red clump and the fourth is consistent with being a blue straggler. The cleaned color-magnitude diagram shows a richly populated red giant branch and a blue straggler population. Half of the blue stragglers are in binaries. From our radial-velocity measurement distribution we find the cluster's radial-velocity dispersion to be  $\sigma_c = 0.62 \pm 0.10 \text{ km s}^{-1}$ . This corresponds to a dynamical mass of  $\sim 4600 M_{\odot}$ .

*Subject headings:* stars: blue stragglers, open clusters and associations: individual: NGC 6791

### 1. INTRODUCTION

Galactic open star clusters are a key laboratory for observationally constraining models of stellar evolution. The open cluster NGC 6791 resides in a sparsely populated area of the age and metallicity parameter space with its unique combination of old age ( $\sim 8$  Gyr; Grundahl et al. 2008) and high metallicity ( $[\text{Fe}/\text{H}] = +0.30$ ; Boesgaard et al. 2009). As such, it has been the subject of many photometric surveys (Kinman 1965; Kaluzny & Rucinski 1995; Stetson et al. 2003; Platais et al. 2011; Carraro et al. 2013), spectroscopic studies (Liebert et al. 1994; Carraro et al. 2006; Boesgaard et al. 2009; Frinchaboy et al. 2013), eclipsing binary studies (Grundahl et al. 2008; Brogaard et al. 2012), variable star surveys (Hartman et al. 2005; Mochejska et al. 2005; de Marchi et al. 2007), and an X-ray binary survey (van den Berg et al. 2013). Falling within the *Kepler* field (Borucki et al. 2010), NGC 6791 also has asteroseismic measurements of select red giant (RG) and red clump (RC) stars (Stello et al. 2011; Corsaro et al. 2012).

With this wealth of data, NGC 6791 has proven difficult to describe in terms of a single-age stellar population. Evidence for extended star formation (Twarog et al. 2011), blue straggler stars (BSSs; Kinman 1965), red stragglers (sub-subgiants; Platais et al. 2011), young white dwarfs (Bedin et al. 2005; Kalirai et al.

2007), and extreme horizontal branch (EHB) and blue-horizontal branch stars in addition to a rich RC (Kaluzny & Udalski 1992; Green et al. 1996) make this open cluster a popular target of observers and theorists alike. The potential presence of EHB stars, for instance, may make NGC 6791 our closest analog in studying the ultraviolet upturn of elliptical galaxies (Buzzoni et al. 2012). With a diversity of stellar sources for study, secure membership determinations remain a foremost priority before extensive future analyses.

The Platais et al. (2011, hereafter P11) proper-motion (PM) study provides the first comprehensive, kinematic membership determination for NGC 6791. A previous PM study by Cudworth & Anthony-Twarog (1993) was limited to only the inner  $3'$ . Other memberships based on radial-velocity (RV) measurements, eclipsing binaries, spectroscopically derived stellar parameters, and/or asteroseismic measurements have, thus far, been limited to small sample sizes.

A surprising finding of the P11 study was a proposed population of 12 horizontal branch stars (7 having proper-motion membership probabilities above 90%) extending blueward continuously from the RC into the BSS domain (hereafter referred to as blue-HB candidates). Given the high metallicity of the cluster ( $[\text{Fe}/\text{H}] = +0.30$ ), core helium-burning stars are expected to reside within the RC, making this seeming horizontal branch an anomaly. Brogaard et al. (2012) point out that in a Johnson *BV* color-magnitude diagram (CMD) a model zero-age horizontal branch is more luminous than the locus of blue-HB stars proposed by P11. Therefore, these authors suggest that the blue-HB candidates must instead be BSSs. Inconsistencies like this motivate our investigation into the nature of these stars using multi-epoch, high-resolution spectroscopy.

<sup>1</sup> Department of Astronomy, University of Wisconsin–Madison, 475 North Charter Street, Madison, WI 53706, USA; tofflemi@astro.wisc.edu

<sup>2</sup> Visiting Astronomer, Kitt Peak National Observatory, National Optical Astronomy Observatory, which is operated by the Association of Universities for Research in Astronomy (AURA) under cooperative agreement with the National Science Foundation.

<sup>3</sup> Department of Physics and Astronomy, The Johns Hopkins University, Baltimore, MD 21218, USA; imants@pha.jhu.edu

Through the WIYN<sup>4</sup> Open Cluster Study (WOCS; Mathieu 2000), we provide the first, high-precision, systematic RV survey of the evolved population of NGC 6791 within 30' of the cluster center. Combining high-precision RV and PM memberships, we define secure, three-dimensional kinematic memberships for a complete stellar sample including RGs, HB stars, and BSSs. Our ongoing survey allows us to also characterize the binary population and determine the cluster's radial-velocity dispersion from which we derive the first dynamical mass estimate for this cluster. Our paper is structured as follows: Section 2 describes our survey sample, Section 3 details our observation and data reduction scheme, and Section 4 presents our observation completeness. Sections 5 and 6 present our results and discussion, respectively, and a summary of our conclusions is provided in Section 7.

## 2. STELLAR SAMPLE

The source catalog for our RV survey of NGC 6791 is drawn from the PM study of P11. In this study, deep photographic plates dating back to 1961 from the Kitt Peak National Observatory (KPNO) 4 m and the Lick 3 m telescopes, along with CCD mosaic frames taken from 1998–2009 with the KPNO 4 m and the 3.6 m Canada-France-Hawaii Telescope (CFHT), were used to obtain high-precision proper motions for 58,901 stars down to  $g' \sim 24$ . Within the 0.8 deg<sup>2</sup> field of view (FOV), a total of 5,699 PM probable cluster members were found based on the chosen cluster membership probabilities combined with certain CMD restrictions (Figure 1 in P11). In general, stars with PM membership probabilities  $P_\mu \geq 19\%$  were taken to be probable cluster members, although a looser constraint of  $P_\mu \geq 1\%$  was used for stars falling on the main sequence. The complete catalog of positions, proper motions, membership probabilities, and  $g'$  and  $r'$  photometry will appear in I. Platais et al. (2014, in preparation).

Our RV catalog is drawn from all P11 sources above a limiting magnitude of  $g' \leq 16.8$ , set by the minimum signal-to-noise ratio required by our survey. They comprise the evolved stellar population including the RG branch (RGB), RC, possible blue-HB stars, and BSSs. We trim the full sample only by excluding  $P_\mu = 0\%$  sources, assuming they are field stars. This assumption is supported by the CMD of  $P_\mu = 0\%$  stars, presented in Figure 1, which lacks apparent cluster features such as the RGB. The CMD membership cut of  $P_\mu \geq 19\%$  used by P11, aimed to minimize the field contamination expected in low- $P_\mu$  sources. In the  $1\% \leq P_\mu < 19\%$  sample, however, some cluster members are indeed expected. Thus, we include them in our RV catalog with the expectation that RV membership information will draw out the cluster members. Applying this selection criterion ( $P_\mu > 0\%$ ) yields a total sample to 280 sources.

## 3. OBSERVATIONS & DATA REDUCTION

Here we briefly present our observing and data reduction procedures. (We refer readers to Geller et al. (2008) for full details.) Variations in our methods from previous WOCS RV papers are given below.

<sup>4</sup> The WIYN Observatory is a joint facility of the University of Wisconsin-Madison, Indiana University, Yale University, and the National Optical Astronomy Observatory.

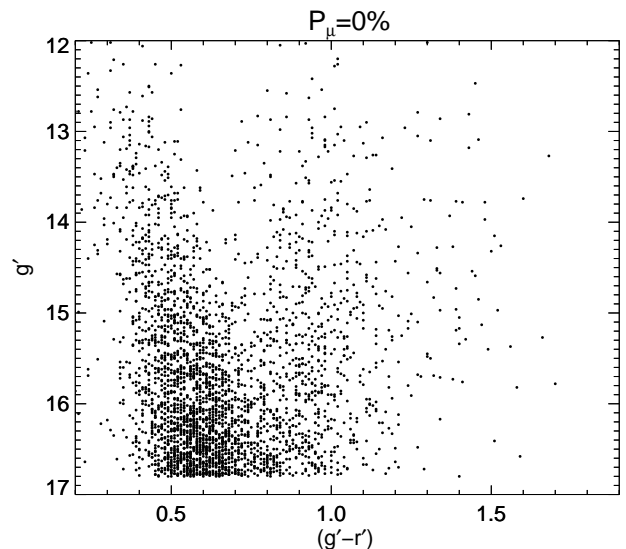


**Figure 1.** CMD of proper-motion-defined field stars ( $P_\mu = 0\%$ ). Signatures of cluster members, like the RGB, are absent. (Compare with Figure 7 below.)

### 3.1. Spectroscopic Observations

Our ongoing spectroscopic survey of NGC 6791 has, to date, yielded 1189 RV measurements of 260 stars. Observations utilize the Hydra Multi-Object Spectrograph (MOS) on the WIYN 3.5 m telescope, capable of obtaining  $\sim 70$  stellar spectra simultaneously over a 1° field of view. We use 3'' diameter fibers along with the bench spectrograph echelle grating, resulting in a spectral resolution of  $\sim 20,000$  ( $15 \text{ km s}^{-1}$ ). Due to the number of source fibers, the echelle grating is not cross-dispersed and the X14 filter is used to isolate the 11th spectral order. This 250 Å-wide region centered at 5125 Å contains many stellar absorption lines including the Mg I b triplet.

To begin our observing program, the catalog is split into bright ( $12 < g' < 15.9$ ) and faint ( $12.9 < g' < 16.8$ ) sub-samples to prevent on-chip contamination between source spectra. Bright and faint Hydra configurations generated from these sub-samples are observed for 1 and 2 hours, respectively, to ensure a sufficient signal-to-noise ratio ( $S/N \simeq 18$  per resolution element under ideal observing conditions for all targets). Integrations are split into three equal exposures to reduce the impact of cosmic ray contamination. Of the 81 available fibers, each configuration observes a maximum of 71 stellar spectra with 10 fibers reserved for sky sampling. As accurate wavelength calibration is vital to this program's success, comparison ThAr emission lamp spectra are taken before and after each configuration to correct for wavelength shifts during the observing sequence. Dome flat-field images are also taken for each configuration to aid in throughput correction and aperture identification during spectral extraction.

Target prioritization aims to efficiently determine the RV membership of proper-motion-selected stars. Monte Carlo (MC) simulations have shown that 3 observations over the course of 200 days can determine, to  $\sim 90\%$  confidence, whether a star has a constant or variable RV for binary orbital periods up to 1000 days (following Geller & Mathieu 2012). As such, for a given ob-

servicing run, we place stars with one observation at the highest priority followed by twice-observed likely members (stars whose first two RV measurements fall within the cluster’s RV distribution), twice-observed likely non-members, unobserved stars, and finally, stars with three or more observations over the course of at least 200 days. The 12 blue-HB candidates from P11 were given the highest priority until their RV memberships were determined. Unlike previous WOCS RV studies, we have not yet chosen to prioritize binary orbit determinations for velocity-variable stars in favor of maximizing the number of single stars with determined RV memberships. Stars with the highest PM probabilities were also prioritized in our observations.

### 3.2. Data Reduction

All WOCS image processing and data reduction are completed using standard IRAF<sup>5</sup> tasks. Our routine is as follows. Bias subtraction from an overscan region is first applied to raw science and flat-field images. Spectral extraction, flat-field correction, throughput correction, and dispersion solutions are computed and applied with the *dohydra* reduction task. Remaining sky fibers are visually inspected for quality and median combined to perform sky subtraction. The three fully reduced spectra from each configuration are then median combined to improve S/N and remove cosmic ray contamination.

Fourier cross-correlation functions (CCF) between stellar spectra and a zero-velocity template are computed using the IRAF task *fxcor*. A Gaussian fit to the CCF peak provides the relative velocity shift between the two spectra, which is then corrected for the Earth’s orbital motion to produce a heliocentric RV. Geller et al. (2008) define a minimum CCF peak height of 0.4 as sufficient correlation for a secure RV measurement utilizing the same observational and data reduction schemes. We adopt this same minimum CCF peak value to identify acceptable RV measurements. Finally, systematic fiber-to-fiber RV offsets derived by Geller et al. (2008) are then applied to the computed heliocentric RV, yielding our final RV measurement.

In the case of double-lined spectroscopic binaries, we are able to retrieve the radial velocities of both stars simultaneously using the two-dimensional correlation routine TODCOR (Zucker & Mazeh 1994). Using a zero-velocity template for each star, we fit a two-dimensional correlation that is able to effectively decompose strongly blended lines. The result of this routine is a heliocentric RV for each star in the system that is then corrected for fiber-fiber variations.

As in previous WOCS surveys, the standard Fourier cross-correlation template is a high-S/N solar spectrum from a sky flat. For most stars in the NGC 6791 sample, a strong correlation peak is found using the solar template. However, a handful of RGs in our sample exhibit the Swan C<sub>2</sub> absorption band near 5165Å that prevents precise RV measurements against a solar template. For this subset, we use the spectrum of the K1 III star, HD172171, from the publicly available ELODIE

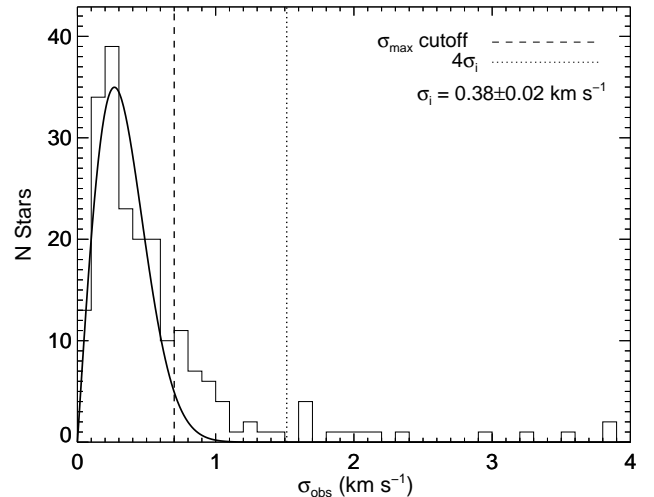


**Figure 2.** Distribution of the standard deviation of the first 3 RV measurements for each star. The solid curve displays the best fit of the  $\chi^2$  model within the  $\sigma_{\max}$  cutoff represented by the dashed vertical line. A best-fit precision of  $\sigma_i = 0.38 \pm 0.02 \text{ km s}^{-1}$  is found. The vertical dotted line marks  $4\sigma_i$ , the minimum standard deviation required for a velocity-variable designation.

Stellar Library (Prugniel & Soubiran 2001) as our template. This spectrum is provided at zero-velocity and is set to a zero-heliocentric-velocity for cross-correlation. Containing the same C<sub>2</sub> absorption feature and at a spectral resolution of  $\sim 42,000$ , we retrieve strong correlation peaks for this subset of RGs in our sample. Additionally, the RV zero-points for cluster members found using the solar and RG template are consistent.

### 3.3. Precision

To assess our measurement precision we fit the standard deviations of RV measurements with a  $\chi^2$  distribution following Geller et al. (2008). For consistency across our sample, we take only objects with at least three observations, and use only the first three RV measurements when calculating standard deviations ( $\sigma_{\text{obs}}$ ). The  $\chi^2$  function models the distribution of error for measurements of single (non-velocity-variable) stars. We fit the following form,

$$\chi^2(\sigma_{\text{obs}}) = A \left( \frac{2}{\sigma_i^2} \right) (\sigma_{\text{obs}}) \exp \left( -\frac{\sigma_{\text{obs}}^2}{\sigma_i^2} \right), \quad (1)$$

with two free parameters:  $A$ , the  $\chi^2$  normalization, and  $\sigma_i$ , our RV measurement precision. The velocity variability of binary stars in our sample inflates the tail of our error distribution with sources of high measurement deviation. To account for this, we fit  $\chi^2$  only to data within a  $\sigma_{\max}$  cutoff to limit binary contamination. Varying  $\sigma_{\max}$  at  $0.1 \text{ km s}^{-1}$  intervals we find that a value of  $\sigma_{\max} = 0.7 \text{ km s}^{-1}$  produces the lowest residuals in the fit and we adopt this value as our cutoff.

Figure 2 presents our empirical RV standard deviations with the best-fit error distribution over-plotted as a solid line. The dashed vertical line signifies the  $\sigma_{\max}$  cutoff. Contamination from velocity variables can be clearly seen exceeding the  $\chi^2$  fit beyond the cutoff. We find a best-fit precision of  $\sigma_i = 0.38 \pm 0.02 \text{ km s}^{-1}$  that is insensitive to

<sup>5</sup> IRAF is distributed by the National Optical Astronomy Observatory, which is operated by the Association of Universities for Research in Astronomy (AURA) under cooperative agreement with the National Science Foundation.

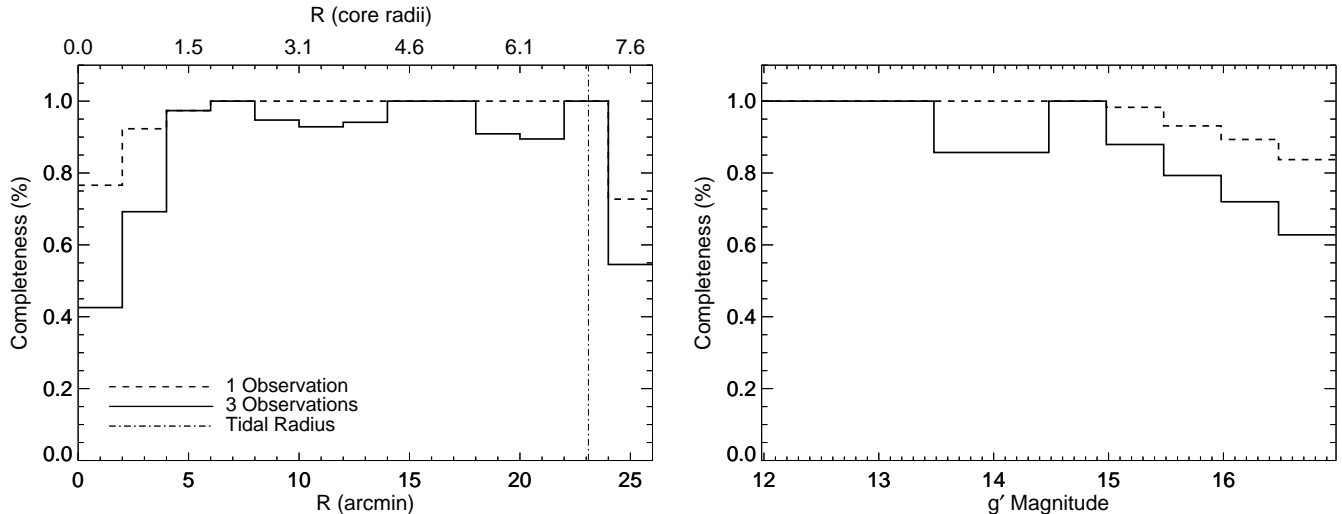


**Figure 3.** Completeness histograms as a function of radius and  $g'$  magnitude for our sample ( $P_\mu \geq 1\%$ ). Dashed lines show the completeness of stars with  $\geq 1$  radial-velocity measurements. Solid lines show the completeness of stars with  $\geq 3$  measurements over the course of at least 200 days (for which we can determine radial-velocity membership). In the left panel we present radius in both arcminutes and core radii for  $R_c = 3.8$  pc (P11) at a distance of 4 kpc (Grundahl et al. 2008). The dot-dashed vertical line marks the tidal radius of the cluster at 23.1 ( $\sim 27$  pc; P11).

the value of  $\sigma_{\max}$  chosen, producing a consistent result for  $\sigma_{\max} = 0.6 - 0.8$  km s $^{-1}$ . Our best-fit measurement precision is consistent with that found in the Geller et al. (2008) study of NGC 188 ( $\sigma_i = 0.4$  km s $^{-1}$ ).

From our RV precision, we define a minimum standard deviation in observed RV for a star to be characterized as a “velocity-variable”. As in Geller et al. (2008), we use the quantity  $e/i$  to define velocity variables where  $e$  is the observed standard deviation of a given star ( $\sigma_{\text{obs}}$ ) and  $i$  denotes our precision ( $\sigma_i$ ). Stars with  $e/i > 4$  are designated as velocity variables. The  $e/i$  limit is plotted as the vertical dotted line in Figure 2, where stars falling right of this line are considered to be velocity variable.

#### 4. COMPLETENESS

By combining precise RV and PM memberships, we seek to define a complete sample of the evolved stellar population within a radius of 30' ( $\sim 35$  pc at  $d = 4$  kpc) from the cluster center. We adopt the Stetson et al. (2003) cluster center in the following analysis ( $\alpha = 19^{\text{h}}20^{\text{m}}53^{\text{s}}$ ;  $\delta = +37^{\circ}46'30''$ ; J2000), which is within 2" from our independent estimate. Within the magnitude range of our sample (see Section 2), there are 280 sources ( $P_\mu \geq 1\%$ ). Of these, 93% have at least one RV measurement and 79% have  $\geq 3$  measurements over the course of at least 200 days. As stated above, we have presumed that stars with  $P_\mu = 0\%$  are securely not cluster members.

Achieving 3 RV measurements over the course of at least 200 days is required to determine, with  $\sim 90\%$  confidence, whether a star is velocity variable. Since RV membership probabilities are only computed for non-velocity-variable stars (Section 5.2), this observational benchmark sets the completeness for which we can determine membership or binarity.

Distributions of RV measurement completeness with respect to radius and  $g'$  magnitude are presented in the left and right panels of Figure 3, respectively. The dashed line represents completeness with  $\geq 1$  measure-

ment. Completeness with  $\geq 3$  measurements over 200 days is shown as the solid line. Radius is given in arcminutes (bottom) and in core radii (top) based on the P11 derivation of  $R_c \simeq 3.8$  pc from King model fitting (King 1966) to the stellar number-density profile (assuming a distance of 4 kpc,  $1'' = 1.16$  pc; Grundahl et al. 2008). The cluster tidal radius ( $\sim 27$  pc; P11) is also presented as the vertical dot-dashed line.

The decline in RV measurement completeness at small radii and at faint magnitudes is due to the same population of dim, centrally concentrated stars. Observations of these stars are limited by the number of Hydra fibers that can be placed in the dense cluster center, compounded with the time expense of obtaining 2 hr exposures for faint stars.

## 5. RESULTS

### 5.1. Radial-Velocity Measurements

The results of our RV survey are summarized in Table 1, where we present 10 lines selected to illustrate the table format and relevant comment and class fields. The full table is available electronically. For each star, we include the WOCS ID ( $\text{ID}_W$ ), R.A. and Declination (J2000),  $g'$  magnitude, and  $(g'-r')$  color from the P11 catalog. The succeeding columns present the number of WIYN RV measurements ( $N_{\text{obs}}$ ), mean RV ( $\overline{\text{RV}}$ ), PM membership probability ( $P_\mu$ ), RV membership probability ( $P_{\text{RV}}$ ),  $e/i$  value, membership class (detailed in Section 5.2), and comments. Both the  $\overline{\text{RV}}$  and  $e/i$  value are calculated using an error-weighted mean. RV membership probabilities in parenthesis indicate a tentative value for velocity variable stars based on their mean RV ( $P_{\text{RV}}$ ), which remains uncertain until a binary orbital solution is found. In the comment field, we highlight the following stars: velocity variables as single- or double-lined spectroscopic binaries (“SB1” and “SB2”, respectively), RGs containing strong C $_2$  absorption for which a KIII stellar template was used (“C $_2$  Band”), BSSs (“BSS”), and finally, rapidly rotating stars (“RR”), defined as having

**Table 1**  
Radial Velocity Summary Table

ID <sub>W</sub>	R.A.	Dec.	$g'$	$g'-r'$	$N_{\text{obs}}$	$\overline{RV}$	$P_{\mu}$	$P_{RV}^a$	$e/i$	Class	Comment
1002	19:20:55.11	37:47:16.3	14.63	1.41	5	-47.51	99	96	0.31	SM	
1003	19:20:50.04	37:47:28.2	13.50	0.95	1	-49.49	10	...	...	U	
1004	19:20:58.63	37:47:40.5	11.99	0.88	3	-13.21	10	0	0.70	SN	
2003	19:20:47.66	37:47:32.3	15.33	1.23	3	-54.20	99	(0)	53.30	BU	SB1
3006	19:20:49.72	37:43:42.7	14.83	1.50	4	-46.47	99	94	1.30	SM	C <sub>2</sub> Band
4003	19:20:59.95	37:46:03.3	15.15	0.28	13	-44.76	99	54	1.62	SM	BSS
6006	19:20:49.65	37:44:07.8	15.18	1.10	3	-49.03	10	(89)	4.26	BLM	SB1
7021	19:20:33.03	37:55:55.9	14.21	1.10	14	-75.11	41	(0)	11.00	BLN	SB1
7045	19:21:22.34	38:07:57.1	14.04	0.39	10	-1.88	37	(0)	3.22	SN	RR (113.1 km s <sup>-1</sup> )
43033	19:22:15.20	37:48:47.2	15.82	0.55	6	-41.70	6	(0)	79.28	BU	SB2

**Note.** — This table is available in its entirety in a machine-readable form in the online journal. A portion is shown here for guidance regarding its form and contents. Photometry, coordinates, and proper-motion membership probabilities come from I. Platais et al (2014, in preparation).

<sup>a</sup> RV membership probabilities in parenthesis indicate the probability of the mean RV for velocity variables ( $P_{\overline{RV}}$ ) and remains uncertain until a binary orbital solution is found.

a CCF FWHM  $\geq 60$  km s<sup>-1</sup>, are presented with their projected  $v \sin i$  rotational velocity in parenthesis.

Stars designated as RR have reduced RV measurement precision due to their broadened photospheric absorption lines and correspondingly broad CCF peaks. The Geller et al. (2010) study of the young open cluster M35 found that RV measurement precision scaled linearly with the projected  $v \sin i$  rotational velocity and had the functional form  $\sigma_i = 0.38 + 0.012(v \sin i)$  km s<sup>-1</sup>. We find that 10 stars in our sample ( $\sim 4\%$ ) are defined as RRs and following Geller et al. (2010), we derive  $v \sin i$  for these stars from their CCF FWHM. The largest  $v \sin i$  found is  $\sim 110$  km s<sup>-1</sup>. For these stars, the  $e/i$  value and velocity-variable designation are computed based on their  $v \sin i$  dependent  $\sigma_i$  value. None of the 10 RRs are RGB or RC stars as expected; however, 3 are binary BSS candidates (see Section 6.3).

Table 2 presents every NGC 6791 RV measurement and CCF peak height obtained with the WIYN telescope through 2014 February. We have included only a selection of the table here for brevity. The full table is available electronically. The right two columns are reserved for SB2s when a velocity and CCF peak height for each star can be obtained.

### 5.2. Radial-Velocity Membership

Calculations of RV membership require a decomposition of the RV distribution into field-star and cluster distributions. To separate these two components, we fit our distribution of RV measurements for the entire sample ( $P_{\mu} \geq 1\%$ ) simultaneously with two Gaussians. Figure 4 presents our RV measurement histogram of single, non-rapidly rotating stars with the best-fit field-star and cluster population models over-plotted in red and blue, respectively. The fit is made to an 80 km s<sup>-1</sup> region centered around the cluster peak. From this procedure, we find a cluster RV of  $-47.40 \pm 0.13$  km s<sup>-1</sup> and RV standard deviation of  $\sigma_{6791} = 1.1 \pm 0.1$  km s<sup>-1</sup>. The true one-dimensional velocity dispersion of the cluster,  $\sigma_c$ , is less than the Gaussian fit  $\sigma_{6791}$  due to inflation from binary contamination and our measurement precision. These issues are addressed in Section 6.4.

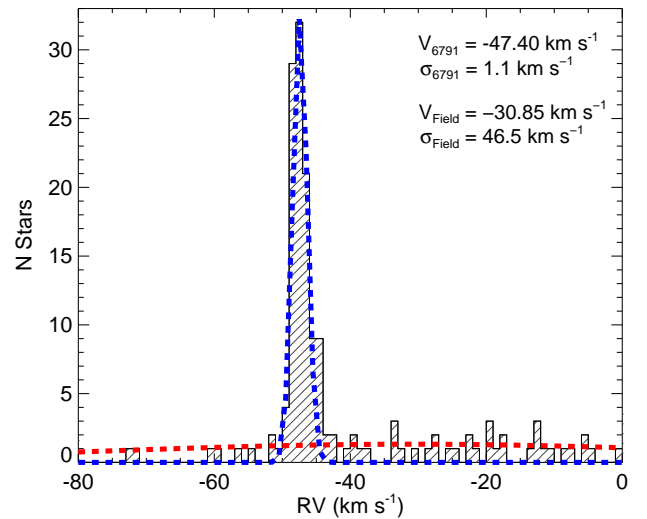


**Figure 4.** Radial-velocity histogram of single, non-rapidly rotating stars. Gaussian fits to the field and cluster RV distributions are over-plotted in red and blue respectively. Top right provides the radial-velocity mean and standard deviation for each of these fits.

With a model of the two populations, we define RV membership with the following equation:

$$P_{RV}(v) = \frac{F_{\text{cluster}}(v)}{F_{\text{field}}(v) + F_{\text{cluster}}(v)}, \quad (2)$$

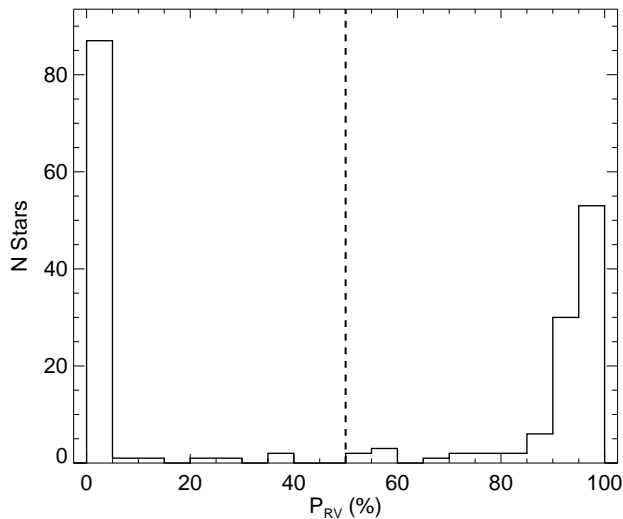
where  $F_{\text{cluster}}(v)$  is the cluster-model value for the stellar RV,  $v$ , and  $F_{\text{field}}(v)$  is the field-star-model value for the same RV (Vasilevskis et al. 1958). We find the field distribution to be well separated from the field velocity center ( $-30.85$  km s<sup>-1</sup>), providing a good separation in membership probability between cluster and field stars.

Figure 5 presents a histogram of our RV membership probabilities for single stars. As noted above, a clear separation is found between cluster members and field stars. In keeping with previous WOCS practice, we set our cutoff for RV membership at  $P_{RV} = 50\%$ , designated by the vertical dashed line.

**Table 2**  
Radial Velocity Data Table

ID <sub>W</sub>	HJD-2,450,000 (days)	RV <sub>1</sub> (km s <sup>-1</sup> )	Correlation Height <sub>1</sub>	RV <sub>2</sub> (km s <sup>-1</sup> )	Correlation Height <sub>2</sub>
1002	5754.679	-47.5	0.63		
	5821.717	-47.4	0.60		
	5995.996	-47.5	0.61		
	6053.821	-47.4	0.60		
	6524.863	-47.7	0.62		
1003	6524.863	-49.5	0.93		
1004	5754.751	-12.9	0.95		
	5821.717	-13.0	0.95		
	6705.980	-13.4	0.95		
43033	5755.698	-31.4	0.75		
	5821.717	-27.1	0.89		
	5995.996	-2.9	0.67	-60.9	0.57
	6052.802	-57.8	0.72	-1.1	0.66
	6524.863	-49.5	0.66	-12.4	0.51
	6705.980	-8.0	0.58	-55.0	0.50

**Note.** — The two right columns are reserved for double-lined spectroscopic binaries when a velocity and CCF peak height can be obtained for each star. This table is available in its entirety in a machine-readable form in the online journal. A portion is shown here for guidance regarding its form and contents.



**Figure 5.** RV membership probability histogram for single stars. We set an RV membership cutoff at 50%, shown by the vertical dashed line.

With our membership scheme established, we use the field distribution presented in Figure 4 to estimate the number of field-star contaminants expected among our RV members. By integrating the model field distribution over RVs producing  $P_{RV} \geq 50\%$ , we expect 7 of our RV members to be field stars.

From our RV membership determination, we define a star’s membership “Class”, given in the penultimate column of Table 1, following Geller et al. (2008). As presented in Section 3.1, MC simulations show that three RV measurements over the course of 200 days can detect, to  $\sim 90\%$  confidence, binaries with orbital periods up to 1000 days. This baseline in time and number of observations is required for membership determination

and as such, any star not meeting this criterion is given an unknown (U) classification in Table 1. A single star ( $e/i \leq 4$ ) meeting these conditions is designated a single member (SM) if  $P_{RV} \geq 50\%$  or a single non-member (SN) if its RV probability falls below this criterion. A velocity-variable star ( $e/i > 4$ ) can fall into three classes: (1) binary likely member (BLM) if the membership probability based on its mean RV ( $P_{\overline{RV}}$ ) exceeds our criterion, (2) binary unknown (BU) if  $P_{\overline{RV}}$  falls below 50% but the range of measured RV crosses the cluster mean, or (3) binary likely non-member (BLN) if the range in measured RV does not cross the cluster mean. Once orbital solutions are found for binary systems,  $P_{RV}$  will be computed based on the center-of-mass velocity. At that point, binary stars will be classified as binary members (BM) or binary non-members (BN) with the same criteria as single stars. Table 3 lists the number of stars falling within each membership class.

### 5.3. Comparison of Proper-Motion and Radial-Velocity Memberships

Of the 280 stars in our sample, 193 are single (non-velocity variable) stars with RV membership determinations. Figure 6 presents the comparison of RV and PM membership probabilities for all single stars. The vertical dashed line marks the RV (50%) membership criterion. All blue-HB candidates from P11 are presented as blue diamonds. Note that some blue-HB candidates are velocity variables and thus are presented as a blue diamond without central points. Their RV membership positions represent the probabilities of their mean RV ( $P_{\overline{RV}}$ ) and are subject to change until an orbital solution is found (see Section 6.2 for full details). In Figure 6, we also present the marginal distributions along each axis in the top and right panels.

Integrating the PM membership probabilities of stars with RV membership determinations (193),  $106 \pm 3$  cluster members are predicted, in good agreement with the

**Table 3**  
Number of Stars Within  
Each Membership Class

Class	$N_{\text{stars}}$
SM	101
SN	92
BLM	10
BU	6
BLN	12
U	59

101 RV members found. Breaking the stars with RV membership determinations into three subsamples based on their PM membership probabilities we find:

- $86 \pm 1$  cluster members out of 89 are predicted in the  $P_{\mu} > 80\%$  sample while 81 RV members are found,
- $17 \pm 2$  cluster members out of 37 are predicted from the  $19\% \leq P_{\mu} \leq 80\%$  sample while 11 RV members are found,
- $3 \pm 1$  cluster members out of 67 are predicted from the  $1\% \leq P_{\mu} < 19\%$  sample while 9 RV members are found.

Generally, we find fewer RV cluster members than the PM membership probabilities would suggest. However, for stars with  $1\% \leq P_{\mu} < 19\%$ , we find  $\sim 6$  more RV members than the PM prediction. Recalling that 7 field stars are expected among our RV members (Section 5.2), it is reasonable to suspect that some of our field contaminants are likely to be drawn from the 9 RV members with  $1\% \leq P_{\mu} < 19\%$ . As such, we note them in our cleaned CMD (gray points; Figure 7(b)).

However, of these 9 low- $P_{\mu}$  RV members 7 fall on the cluster RGB or RC in the cleaned CMD. Based on the CMD distribution of the 67 stars with  $1\% \leq P_{\mu} < 19\%$  and RV membership determinations, a random draw of 9 such stars would predict only one to fall in the RGB/RC region. For this reason we suspect that most of these 9 stars are in fact cluster members and include them with equal significance in our analyses below.

## 6. DISCUSSION

### 6.1. Color-Magnitude Diagram

Three-dimensional kinematic membership determinations using both PM and RV measurements allow us to construct a cleaned CMD for the evolved population of NGC 6791. Figure 7(a) displays the PM probable members ( $P_{\mu} \geq 19\%$ ) within our magnitude limit as black circles, with the 12 blue-HB candidates marked in blue diamonds. Stars with  $P_{\mu} < 19\%$  are shown as light-gray points. The addition of RV membership information produces Figure 7(b) and represents the most secure, systematic membership determination to date for this cluster. In this lower panel, single members (SMs) are marked as black points. Circled points signifying binary likely members (BLMs).

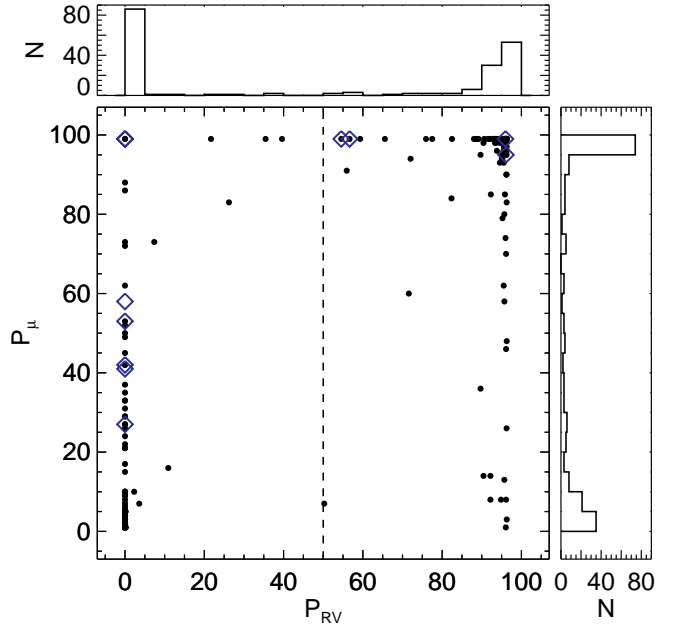


**Figure 6.** A comparison of the P11  $P_{\mu}$  values (y-axis) with our  $P_{RV}$  values (x-axis) for single stars. The dashed vertical line represents the radial-velocity membership criterion (50%). The blue-HB candidates from P11 are highlighted in blue diamonds. Blue diamonds without a central point are velocity variable. Their radial-velocity membership position reflects the membership probability of their mean radial velocity. Marginal distributions along each axis are presented in the top and right panels.

In Figure 7(b), we also include 3 candidate binary members falling near the BSS population as gray “ $\otimes$ ” symbols. Although these stars are currently listed as BUs or BLNs in Table 1, based on their RV measurements to date, we feel they have a high likelihood of becoming members once orbital solutions are found. The two BUs (WOCS 54008 and 62041) have large RV variations and few observations, which we suspect are short-period binaries whose mean RV bears little significance on their RV memberships. The other is a BLN (WOCS 46008) whose mean RV is within  $3\sigma$  of the cluster mean velocity. Due to the astrophysical significance of binary stars to the formation of BSSs (see Section 6.3), we note them here for completeness but do not include them in the analysis below.

The lower panel of Figure 7 reveals a richly populated RGB and RC with 97 SM and BLM stars. We find an RG/RC binary fraction of 6.2% for orbits up to 1000 days, assuming that all BLMs are indeed members (fraction not corrected for detection incompleteness). This binary fraction is less than the global RG/RC binary fraction due to our insensitivity to long-period binaries. Additionally, it is likely not representative of the main sequence binary population given that the increased radii of post-main sequence stars will alter or envelop the orbits of close binary companions. (We have not included the 3 blue-HB candidates found just to the blue of the RC in the above analysis, but we comment on them in Section 6.2.)

The width of the RGB is roughly  $(g'-r') \sim 0.2$  mag, broader than expected for a single-age stellar population. Brogaard et al. (2012) derived a differential red-

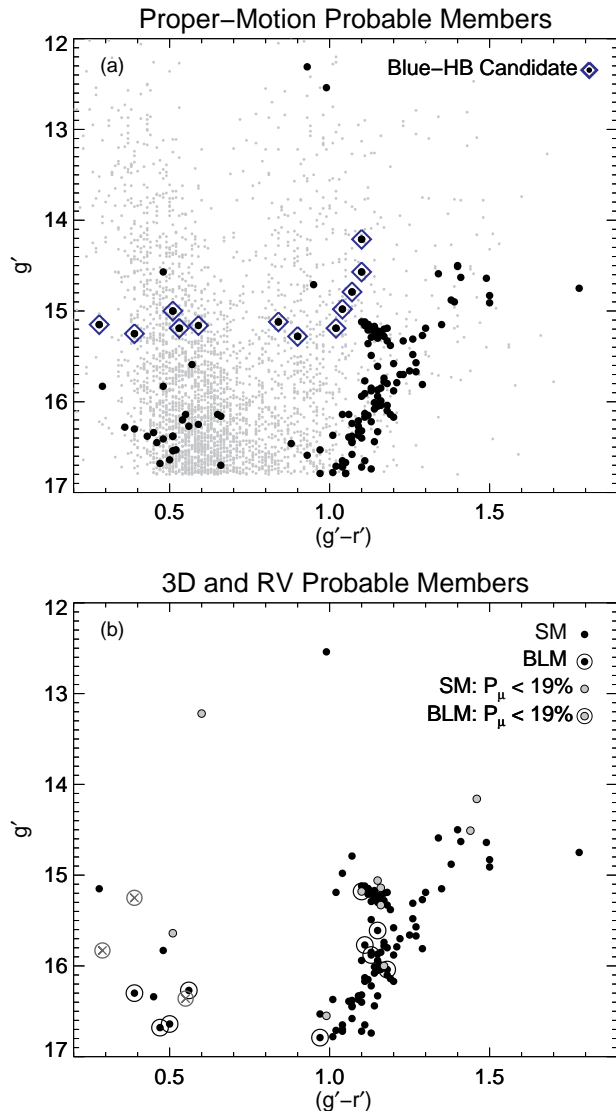


**Figure 7.** (a) Upper CMD of proper-motion probable members ( $P_\mu \geq 19\%$ ) from P11 with blue-HB candidates highlighted in blue diamonds. Small light-gray points are stars with  $P_\mu < 19\%$ . (b) CMD including radial-velocity membership determinations. Single members (SMs) are shown as black points, circled points indicate binary likely members (BLMs). Gray points are SMs and BLMs with  $1\% \leq P_\mu < 19\%$ . Gray “ $\otimes$ ” symbols mark candidate binary members currently classified as binary unknowns (BUs) or binary likely non-members (BLNs), discussed in Section 6.1.

dening map that, when applied on a star-by-star basis, significantly narrowed the RGB.

With the RG/RC and BSS populations well defined, we empirically classify BSSs within our sample as members falling blue of  $(g'-r') = 0.7$ . We designate 8 SM and BLM stars as BSSs and find 4 to be velocity-variable. The BSS population is discussed further in Section 6.3.

Three stars in our CMD are assign to neither the RG/RC nor BSS population. They are the two brightest, WOCS 57012 (SM;  $P_{RV} = 55\%$ ,  $P_\mu = 91\%$ ) and 58012 (RV member only;  $P_{RV} = 92\%$ ,  $P_\mu = 14\%$ ), and the reddest, WOCS 9018 (SM;  $P_{RV} = 95\%$ ,  $P_\mu = 79\%$ ), stars on the cleaned CMD (Figure 7(b)). Their CMD locations are not predicted by any phase of stellar evolution at the age of NGC 6791, nor do we know of similarly located

members in other open clusters. Even given our typically high RV membership probabilities, field contamination cannot be ruled out. Indeed, as noted earlier, our membership probability model (Figure 4) predicts 7 field contaminants among the RV members.

### 6.2. Blue-Horizontal Branch Candidates

Table 4 summarizes our RV membership results for the 12 blue-HB candidates from P11. Here we provide the WOCS IDs ( $ID_W$ ) with a cross reference to the ID given in P11 ( $ID_{P11}$ ) in the first two columns. We find four of these stars we find to be SMs. Three (WOCS 2001, 23004, 15007) fall just to the blue of the RC (see CMD in Figure 7(b)) and the fourth, WOCS 4003, is the bluest star in the cleaned CMD, lying in the BSS regime.

Of the remaining 8 blue-HB candidates, 5 are single stars that are RV non-members ( $P_{RV} = 0$ ). Two, while velocity variable (BLN), have mean velocities far from the cluster mean; with a minimum of 12 RV measurements for each, we conclude that they are also RV non-members. The last blue-HB candidate, WOCS 46008, is a velocity variable, rapid rotator listed as a BLN in Table 1. With a mean RV  $2.7\sigma$  ( $6.5 \text{ km s}^{-1}$ ) from the cluster mean velocity we consider it a potential binary member and include it in Figure 7 as the brightest gray “ $\otimes$ ” symbol in the BSS region of the CMD. An orbital solution will be required to securely determine this star’s RV membership.

The results of our RV membership study do not support the presence of a continuous blue-HB population suggested by P11. Instead, we find 1 SM to reside with BSSs in the CMD and 3 SMs that fall just blue of the RC. This observational finding is consistent with the Brogaard et al. (2012) theoretical conclusion that a blue-HB, if one were to exist, would be more luminous than the P11 proposed candidates.

Even so, the three SMs falling near, but to the blue of, the RC remain puzzling as they cannot be explained by the typical photometric error ( $\sim 0.02 \text{ mag}$ ). Although our field-star and cluster population model predicts 7 field contaminants in Figure 7(b), these 3 stars have high PM and RV membership probabilities (Table 4), leaving a small chance that all 3 are field stars.

We speculate that these 3 may be evolved descendants of BSSs. If, for simplicity, we model these stars with normal stellar evolutionary tracks, we find that all three lie on the giant branch of a 1.3 Gyr isochrone, implying masses of  $\sim 2 M_\odot$ . (Here we use a reddening of  $E(g'-r') = 0.165$ , an extinction of  $A_{g'} = 0.65 \text{ mag}$ , an age of 8 Gyr,  $[\text{Fe}/\text{H}] = +0.30$  (Boesgaard et al. 2009), and a distance of 3.8 kpc, obtained by matching Padova isochrones (Bressan et al. 2012) to the NGC 6791 RC and RGB.) This stellar mass is roughly 75% more massive than a typical NGC 6791 giant ( $1.2 M_\odot$ ; Basu et al. 2011). Such a mass is not unprecedented for a BSS, which in this case would have formed  $\sim 1 \text{ Gyr}$  ago. We note that it is surprising that all 3 stars do not have detected velocity variability given the high BSS binary fraction found in NGC 6791 (Section 6.3) and in other open clusters (Geller & Mathieu 2012). This may point to stellar collisions or mergers as the formation mechanism of our evolved BSSs candidates (Leigh & Sills 2011).

The SM status of our fourth blue-HB candidate, WOCS 4003 (2-17; Kinman 1965), confirms the mem-

**Table 4**  
NGC 6791 Blue-HB Proper-Motion Candidate Members

ID <sub>W</sub>	ID <sub>P11</sub>	R.A.	Dec.	$g'$	$g'-r'$	$P_\mu$	$\overline{RV}$ (km s <sup>-1</sup> )	$\sigma_{RV}$ (km s <sup>-1</sup> )	$P_{RV}$ <sup>a</sup>	Comment <sup>b</sup>
23004	69976	19:20:46.00	37:47:54.8	14.98	1.04	95	-47.04	0.34	96	2-45
2001	65895	19:20:51.37	37:46:30.5	14.79	1.07	99	-47.86	0.34	95	NW-20
15007	60456	19:21:07.20	37:44:34.7	15.19	1.02	99	-44.80	0.51	56	3-27
4003	64589	19:20:59.95	37:46:03.3	15.15	0.28	99	-44.76	0.62	54	2-17
46008	64067	19:20:34.98	37:45:52.3	15.25	0.39	99	-40.89	5.29	(0)	S2746; RR; SB1
7021	89107	19:20:33.03	37:55:55.9	14.21	1.10	41	-75.11	4.18	(0)	S2382; SB1
8031	93625	19:21:42.32	37:58:05.5	15.16	0.59	58	-18.89	4.25	(0)	SB1
18007	58857	19:21:02.55	37:43:59.5	15.19	0.53	99	15.57	0.81	0	3-22
9007	69734	19:21:08.07	37:47:49.4	14.57	1.10	99	-22.84	0.33	0	3-33
21016	82982	19:21:14.70	37:53:07.5	15.28	0.90	53	11.47	0.29	0	S14140
19018	52460	19:20:17.44	37:41:23.9	15.12	0.84	42	10.05	0.29	0	S440
11019	45106	19:20:31.40	37:38:09.7	15.00	0.51	27	-54.49	0.28	0	S2101

**Note.** — Photometry, coordinates, and proper-motion membership probabilities come from I. Platais et al (2014, in preparation).

<sup>a</sup> RV membership probabilities in parenthesis indicate the probability of the mean RV for velocity variables ( $P_{\overline{RV}}$ ) and remains uncertain until a binary orbital solution is found.

<sup>b</sup> Stetson et al. (2003) IDs are preceded by an “S”, remaining IDs are from Kinman (1965). SB1 marks single lines spectroscopic binaries, RR marks rapid rotators.

bership first proposed by Green et al. (1996) as a blue-HB star. A subsequent analysis of this star by Brogaard et al. (2012), however, found its spectral properties to be most consistent with a mass of  $1.9 M_\odot$ , whereas the expected mass of an HB star is  $\sim 0.6 M_\odot$ . The large mass along with low luminosity (for a blue-HB star) led these authors to conclude a BSS classification.

Again assuming standard stellar evolutionary tracks, we find this star to lie on a  $\sim 0.9$  Gyr isochrone with a mass of  $\sim 2 M_\odot$ . We conclude (in agreement with Brogaard et al. 2012) that WOCS 4003 is a BSS member that formed perhaps  $\sim 1$  Gyr ago. Given the large mass and non-varying RV, this BSS may also be a candidate for formation via a merger or collision.

### 6.3. Blue Stragglers

Table 5 presents the membership information for BSS members and candidate members. We break our BSS sample into two groups based on their membership likelihood. First, as ordered in Table 5, are SMs and BLMs, totaling 8 stars. The second is comprised of 3 potential BSS members, all velocity variables (BU and BLN), whose large amplitude of variability ( $e/i > 4$ ) and small number of RV measurements make their RV memberships uncertain. We suspect these stars may be cluster members. They are plotted as gray “⊗” symbols in the BSS region of Figure 7(b).

We note that 1 BLM BSS (WOCS 58008) and 2 binary BSS candidates (WOCS 46008, 54008) are designated as rapid rotators. While orbital solutions are still required to confirm the membership of these stars, the distribution of BSS rotation rates may prove to be a valuable test of BSS formation theories (Sills et al. 2005).

Observations to date yield an NGC 6791 BSS population of 8 stars, 4 being SMs and 4 being BLMs. Among the 8 BSS SMs and BLMs, we find a binary fraction of 50% for binaries with orbits up to 1000 days, assuming that all the BLMs are indeed members. The three candidate BSSs would only increase this binary frequency. This is higher than both the RG/RC binary frequency

found above and the main sequence binary fraction determined by the Janes & Kassis (1997) analysis of the CMD binary main sequence (14%). Although still preliminary, the high binary fraction of NGC 6791 BSSs agrees with the findings of Geller & Mathieu (2012) for NGC 188 BSSs ( $76 \pm 19\%$ ). This suggests that binaries may play a key role in the formation of BSSs in NGC 6791. A complete analysis of the binary BSS orbital solutions is required before determining the roles of any specific BSS formation mechanism.

### 6.4. Dynamical Mass

Our systematic RV survey finds  $\sigma_{6791} = 1.1 \pm 0.1$  km s<sup>-1</sup> from our Gaussian fitting procedure (Section 5.2). However, undetected binaries in our sample broaden the wings of the RV distribution and inflate our observed dispersion value. Thus, this Gaussian-fit RV dispersion is an upper limit.

Modeling the effects of binarity on the observed RV dispersion is beyond the scope of this paper. Instead, we use the normal probability plot (Chambers et al. 1983) to derive a measure of the observed RV dispersion that is less sensitive to the wings of the distribution. The normal probability plot in Figure 8 compares our mean RV measurements for single stars (open circles) to a normal distribution. Measurements drawn from a normal distribution map into a straight line whose inverse slope corresponds to the standard deviation of the parent distribution, which in this case is the observed RV dispersion (before correction for measurement errors).

Using the same RV center from our Gaussian fit (Section 5.2), denoted by the dashed vertical line, we fit a line to the central  $1.4$  km s<sup>-1</sup> (vertical dotted lines). We justify fitting to only this central region because this range of data is normally distributed. Fits to more centralized regions reproduce the same result with larger error. Outside this range, it is clear the RV measurements deviate from Gaussian, possibly from binary contamination. Our best-fit line yields an observed RV dispersion of  $0.73 \pm 0.09$  km s<sup>-1</sup>. We then deconvolve the best fit RV dispersion with our measurement precision ( $0.38$  km

**Table 5**  
NGC 6791 Blue Straggler Membership

ID <sub>W</sub>	R.A.	Dec.	$g'$	$g'-r'$	$P_\mu$	$\overline{RV}$ (km s <sup>-1</sup> )	$\sigma_{RV}$ (km s <sup>-1</sup> )	$P_{RV}$ <sup>a</sup>	Comment <sup>b</sup>
Single Members & Binary Likely Members									
4003	19:20:59.95	37:46:03.3	15.15	0.28	99	-44.76	0.62	54	Blue-HB Can.
21028	19:21:56.64	37:52:05.8	15.64	0.51	8	-46.06	1.04	92	
33025	19:19:52.07	37:48:31.6	16.34	0.45	60	-45.10	0.97	71	
70011	19:21:12.68	37:49:48.7	15.83	0.48	97	-47.02	0.37	96	
11003	19:20:58.31	37:47:08.1	16.64	0.50	99	-46.07	1.59	(92)	SB1
22004	19:21:01.05	37:47:34.7	16.68	0.47	99	-48.21	3.77	(95)	SB1
57009	19:20:53.91	37:42:26.0	16.27	0.56	99	-49.62	2.11	(75)	SB1
58008	19:20:10.42	37:47:42.1	16.30	0.39	99	-47.76	5.08	(96)	SB1, RR
Candidates									
46008	19:20:34.98	37:45:52.3	15.25	0.39	99	-40.05	4.39	(0)	SB1, RR, Blue-HB Can.
54008	19:21:10.71	37:45:31.4	15.83	0.29	99	-55.34	10.99	(0)	SB1, RR
62041	19:21:57.88	37:30:56.9	16.36	0.55	2	-53.01	28.80	(0)	SB1

**Note.** — Photometry, coordinates, and proper-motion membership probabilities come from I. Platais et al (2014, in preparation).

<sup>a</sup> RV membership probabilities in parenthesis indicate the probability of the mean RV for velocity variables ( $P_{\overline{RV}}$ ) and remains uncertain until a binary orbital solution is found.

<sup>b</sup> SB1 marks single lines spectroscopic binaries, RR marks rapid rotators.

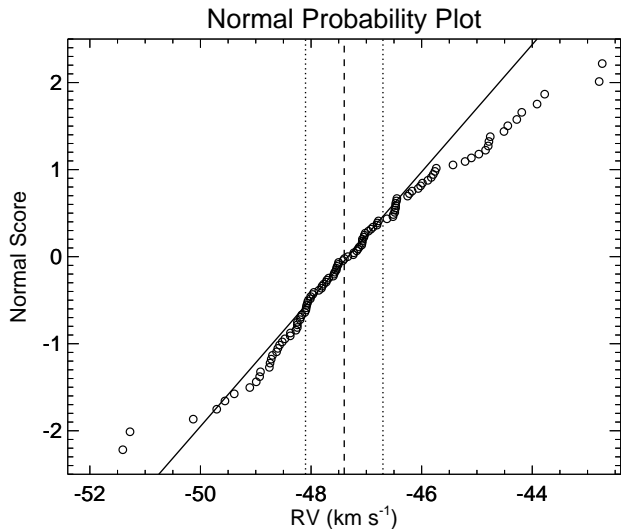


**Figure 8.** Normal probability plot of the mean radial-velocity for single stars. The vertical dashed line marks the cluster mean velocity from Figure 4. The solid line is a linear best-fit to the data within the central 1.4 km s<sup>-1</sup> represented by vertical dotted lines. The inverse slope of this line is a measure of the observed cluster radial-velocity dispersion, yielding  $0.73 \pm 0.09$  km s<sup>-1</sup>.

s<sup>-1</sup>) to obtain a true one-dimensional velocity dispersion of  $\sigma_c = 0.62 \pm 0.10$  km s<sup>-1</sup>.

We calculate the cluster mass using the equation for dynamical mass in projection from Spitzer (1987),

$$M = \frac{10 \langle \sigma_c^2 \rangle R_h}{G}, \quad (3)$$

where  $\sigma_c$  is the one-dimensional velocity dispersion of the cluster and  $R_h$  is the projected half-mass radius. Equation 3 assumes a gravitational potential energy prefactor of 0.4, the observed (projected) half-mass radius measured,  $R_h$ , is 3/4 of the true half-mass radius, and  $\sqrt{3}\sigma_c = \sigma_{3D}$  (Spitzer 1987).

Using  $R_h = 5.1 \pm 0.2$  pc from King model fitting (P11), we find a mass of  $4600 \pm 1500 M_\odot$ . Current literature values for the mass of NGC 6791 based on photometry range from  $\geq 4000 M_\odot$  (Kaluzny & Udalski 1992) to  $\sim 5000 M_\odot$  (P11), in good agreement with our dynamical mass determination. In the context of other open clusters, our derived mass places NGC 6791 in the top 5% of the Piskunov et al. (2008) open cluster sample, complete to 850 pc.

## 6.5. Stars of Note

### 6.5.1. WOCS 54008

WOCS star 54008 is currently listed as a rapidly rotating ( $v \sin i = 67.2$  km s<sup>-1</sup>) SB1 with unknown membership (BU) and a  $P_\mu = 99\%$ . In Figure 7 it is the bluest candidate binary member shown with a gray “⊗” symbol. Mochejska et al. (2005) find this source (V106) to be an eclipsing W UMa type contact system with a period of 1.4464 days. In our CMD, we would consider WOCS 54008 to be a BSS if its membership is confirmed.

W UMa BSSs have been found in open clusters (M 67, S1036; Sandquist & Shetrone 2003) and globular clusters (M 30, 12005407B; Lovisi et al. 2013), pointing to mass transfer as a mechanism for the formation of at least some BSSs. While W UMa-type systems have been found with both decreasing (Qian et al. 2013) and increasing (Christopoulou & Papageorgiou 2013) orbital periods, either the eventual coalescence or detached binary result is predicted to form a BSSs (Qian et al. 2006).

### 6.5.2. WOCS 43033

An SB2 categorized as a BU, WOCS 43033 has RV measurements that cross the cluster mean velocity and a  $P_\mu = 6\%$ . Given its membership class and CMD location ( $g' = 15.82$ ;  $g'-r' = 0.55$ ), WOCS 43033 would normally be placed in the candidate BSS section. Several observations of this system were obtained at phases when the primary and secondary CCF peaks were superimposed. Observations of superimposed peaks reveals an estimate

of the center-of-mass velocity of the system, measured to be  $\sim -27 \text{ km s}^{-1}$ . Although this method is not as precise as measuring the center-of-mass velocity from a full orbital solution, the resulting RV is sufficiently far from the cluster mean of  $-47.40 \text{ km s}^{-1}$  that cluster membership is unlikely. Therefore, WOCS 43033 is neither listed in Table 5 as a candidate BSS nor shown in Figure 7(b) with a gray “ $\otimes$ ” symbol. Nonetheless, observations will continue in order to obtain a full orbital solution and definitively determine its RV membership probability.

### 6.5.3. WOCS 54034

Similar to WOCS 43033 above, WOCS 54034 is an SB2 that falls in the BSS region of the CMD. It has a  $P_\mu = 33\%$  and is classified as a BU from our RV measurements. We determine the center-of-mass velocity of this system to be  $\sim -32 \text{ km s}^{-1}$  from observations with superimposed primary and secondary CCF peaks. Due to its large separation from the cluster mean velocity, we find WOCS 54034’s RV membership unlikely and, for this reason, we exclude it from Figure 7 and Table 5. Observations of this star will continue until an orbital solution is found.

### 6.5.4. Kepler Selected Targets

Stello et al. (2011), using Fourier analysis of *Kepler* lightcurves, determined an asteroseismic membership criterion based on the average large frequency separation,  $\Delta\nu$ , and frequency of maximum oscillation power,  $\nu_{\text{max}}$ . These authors find 65 seismic RG/RC members and 3 probable or uncertain members. A cross reference between our catalogs finds 100% agreement between the three-dimensional kinematic and seismic membership results for the 48 sources (2 are BLMs) which have RV membership determinations. In addition, we find KIC 2437171 (WOCS 3006), which is blended on the *Kepler* CCD, and potential member KIC 2438421 (WOCS 43010) to be SMs.

Continued *Kepler* monitoring of the Stello et al. (2011) vetted targets by Corsaro et al. (2012) established stellar mass and radius estimates as well as distinguished between RG (H-shell burning) and RC (He-core burning) stars. Four stars from this analysis were deemed outliers based on inconsistencies between their determined mass and/or energy production mechanism (H-shell/He-core) and their CMD locations. We comment on the membership on these stars below:

KIC 2437589 (WOCS 16007). This star is classified as an SM with  $P_\mu = 99\%$  and  $P_{\text{RV}} = 91\%$ . On the CMD, this star falls in the RC but has the asteroseismic properties of a massive  $1.7 M_\odot$  RG, whereas the mass of typical NGC 6791 RGB stars is  $1.2 M_\odot$  (Basu et al. 2011). Brogaard et al. (2012) has suggested that this star is an evolved BSS in the RG phase.

KIC 2436417 (WOCS 41008). A SM with  $P_\mu = 99\%$  and  $P_{\text{RV}} = 95\%$ , this star has the same mass and asteroseismic properties as other RC stars, but with a larger radius. This is a proposed “evolved RC star” on its way to the asymptotic giant branch. The larger radius is also consistent with the P11 CMD location as one of the brightest RC stars.

KIC 2437804 (WOCS 4004). Also a proposed evolved RC star, this star has  $P_\mu = 99\%$  and  $P_{\text{RV}} = 89\%$ . This star is also one of the brightest RC stars.

KIC 2437103 (WOCS 3003). With only 2 RV measurements, this star is labeled as unknown (U) in Table 1. The mean of its two RV measurements ( $-49.0$  and  $-49.2 \text{ km s}^{-1}$ ) meet the RV membership criterion ( $P_{\text{RV}} = 87\%$ ) and it has a  $P_\mu = 10\%$ . This star is of note because it falls on the RGB with the asteroseismic properties of an RC star.

## 7. CONCLUSIONS

This program marks the first systematic, high-precision ( $\sim 0.38 \text{ km s}^{-1}$ ) RV survey of the old, metal-rich open cluster NGC 6791. Combining our RV information with proper-motion memberships from I. Platais et al. (2014, in preparation), we derive three-dimensional kinematic membership probabilities for 193 stars. The resulting members define the evolved population of the cluster. Here, we list the main findings of our work.

- We find 91 single cluster members and 6 binary likely members in the RGB and RC.
- Of the 12 blue-HB candidates suggested by Platais et al. (2011) we find 4 to be single cluster members. Three fall just blue of the RC, which we speculate may be evolved BSSs. The last we conclude to be a BSS. Evidence for a blue-HB population is not supported by our RV membership study.
- Four single members and 4 binary likely members are classified as BSSs. Three additional binaries with large velocity variability (short period) may prove to be BSS cluster members once orbital solutions are found.
- We find a 6.2% RG binary frequency and a 50% BSS binary frequency, assuming all binary likely members are indeed members.
- The radial velocity of NGC 6791 is  $-47.40 \pm 0.13 \text{ km s}^{-1}$ .
- With normal probability analysis of our radial-velocity measurement distribution we find a cluster RV dispersion of  $\sigma_c = 0.62 \pm 0.10 \text{ km s}^{-1}$ . This corresponds to a dynamical mass of  $4600 \pm 1500 M_\odot$ .

Our RV survey of NGC 6791 from the WIYN telescope remains ongoing to complete membership statistics, determine orbital solutions for binaries, and investigate the anomalous cluster members of our cleaned CMD including BSSs and potential evolved BSSs.

The authors thank E. Leiner and K. Milliman for many nights of observing and hours of data reduction for this project. We also thank the referee for a thorough read of our paper and helpful comments. Support for this program is provided by NSF grant AST-0908082.

## REFERENCES

- Basu, S., Grundahl, F., Stello, D., et al. 2011, ApJ, 729, L10  
 Bedin, L. R., Salaris, M., Piotto, G., et al. 2005, ApJ, 624, L45

- Boesgaard, A. M., Jensen, E. E. C., & Deliyannis, C. P. 2009, *AJ*, 137, 4949
- Borucki, W. J., Koch, D., Basri, G., et al. 2010, *Science*, 327, 977
- Bressan, A., Marigo, P., Girardi, L., et al. 2012, *MNRAS*, 427, 127
- Brogaard, K., VandenBerg, D. A., Bruntt, H., et al. 2012, *A&A*, 543, A106
- Buzzoni, A., Bertone, E., Carraro, G., & Buson, L. 2012, *ApJ*, 749, 35
- Carraro, G., Buzzoni, A., Bertone, E., & Buson, L. 2013, *AJ*, 146, 128
- Carraro, G., Villanova, S., Demarque, P., et al. 2006, *ApJ*, 643, 1151
- Chambers, K., Cleveland, W., Tukey, P., & Kleiner, B. 1983, *Graphical Methods for Data Analysis* (Belmont, CA, Wadsworth)
- Christopoulou, P.-E., & Papageorgiou, A. 2013, *AJ*, 146, 157
- Corsaro, E., Stello, D., Huber, D., et al. 2012, *ApJ*, 757, 190
- Cudworth, K. M., & Anthony-Twarog, B. J. 1993, in *Bulletin of the American Astronomical Society*, Vol. 25, American Astronomical Society Meeting Abstracts, 110.05
- de Marchi, F., Poretti, E., Montalto, M., et al. 2007, *A&A*, 471, 515
- Frinchaboy, P. M., Thompson, B., Jackson, K. M., et al. 2013, *ApJ*, 777, L1
- Geller, A. M., & Mathieu, R. D. 2012, *AJ*, 144, 54
- Geller, A. M., Mathieu, R. D., Braden, E. K., et al. 2010, *AJ*, 139, 1383
- Geller, A. M., Mathieu, R. D., Harris, H. C., & McClure, R. D. 2008, *AJ*, 135, 2264
- Green, E. M., Liebert, J., & Peterson, R. C. 1996, in *Astronomical Society of the Pacific Conference Series*, Vol. 92, *Formation of the Galactic Halo...Inside and Out*, ed. H. L. Morrison & A. Sarajedini, 184
- Grundahl, F., Clausen, J. V., Hardis, S., & Frandsen, S. 2008, *A&A*, 492, 171
- Hartman, J. D., Stanek, K. Z., Gaudi, B. S., Holman, M. J., & McLeod, B. A. 2005, *AJ*, 130, 2241
- Janes, K., & Kassis, M. 1997, in *Astronomical Society of the Pacific Conference Series*, Vol. 130, *The Third Pacific Rim Conference on Recent Development on Binary Star Research*, ed. K.-C. Leung, 107
- Kalirai, J. S., Bergeron, P., Hansen, B. M. S., et al. 2007, *ApJ*, 671, 748
- Kaluzny, J., & Rucinski, S. M. 1995, *A&AS*, 114, 1
- Kaluzny, J., & Udalski, A. 1992, *Acta Astron.*, 42, 29
- King, I. R. 1966, *AJ*, 71, 64
- Kinman, T. D. 1965, *ApJ*, 142, 655
- Leigh, N., & Sills, A. 2011, *MNRAS*, 410, 2370
- Liebert, J., Saffer, R. A., & Green, E. M. 1994, *AJ*, 107, 1408
- Lovisi, L., Mucciarelli, A., Lanzoni, B., et al. 2013, *ApJ*, 772, 148
- Mathieu, R. D. 2000, in *Astronomical Society of the Pacific Conference Series*, Vol. 198, *Stellar Clusters and Associations: Convection, Rotation, and Dynamos*, ed. R. Pallavicini, G. Micela, & S. Sciortino, 517
- Mochejska, B. J., Stanek, K. Z., Sasselov, D. D., et al. 2005, *AJ*, 129, 2856
- Piskunov, A. E., Schilbach, E., Kharchenko, N. V., Röser, S., & Scholz, R.-D. 2008, *A&A*, 477, 165
- Platais, I., Cudworth, K. M., Kozhurina-Platais, V., et al. 2011, *ApJ*, 733, L1
- Prugniel, P., & Soubiran, C. 2001, *A&A*, 369, 1048
- Qian, S., Yang, Y., Zhu, L., He, J., & Yuan, J. 2006, *Ap&SS*, 304, 25
- Qian, S.-B., Liu, N.-P., Liao, W.-P., et al. 2013, *AJ*, 146, 38
- Sandquist, E. L., & Shetrone, M. D. 2003, *AJ*, 125, 2173
- Sills, A., Adams, T., & Davies, M. B. 2005, *MNRAS*, 358, 716
- Spitzer, L. 1987, *Dynamical evolution of globular clusters* (Princeton, NJ, Princeton University Press, 1987, 191 p.)
- Stello, D., Meibom, S., Gilliland, R. L., et al. 2011, *ApJ*, 739, 13
- Stetson, P. B., Bruntt, H., & Grundahl, F. 2003, *PASP*, 115, 413
- Twarog, B. A., Carraro, G., & Anthony-Twarog, B. J. 2011, *ApJ*, 727, L7
- van den Berg, M., Verbunt, F., Tagliaferri, G., et al. 2013, *ApJ*, 770, 98
- Vasilevskis, S., Klemola, A., & Preston, G. 1958, *AJ*, 63, 387
- Zucker, S., & Mazeh, T. 1994, *ApJ*, 420, 806